Ferroptosis as a Potential Therapeutic Target for Reducing Inflammation and Corneal Scarring in Bacterial Keratitis

Qiankun Chen, Leying Wang, Yuan Wei, Xizhan Xu, Xiaoyan Guo, and Qingfeng Liang

Beijing Institute of Ophthalmology, Beijing Tongren Eye Center, Beijing Tongren Hospital, Capital Medical University, Beijing Key Laboratory of Ophthalmology and Visual Sciences, Beijing, China

Correspondence: Qingfeng Liang, Beijing Institute of Ophthalmology, Beijing Tongren Eye Center, Beijing Tongren Hospital, Capital Medical University, Beijing Key Laboratory of Ophthalmology and Visual Sciences, Beijing 100005, China; lqflucky@163.com.

Received: September 7, 2023
Accepted: February 3, 2024
Published: February 21, 2024

Citation: Chen Q, Wang L, Wei Y, Xu X, Guo X, Liang Q. Ferroptosis as a potential therapeutic target for reducing inflammation and corneal scarring in bacterial keratitis. *Invest Ophthalmol Vis Sci.* 2024;65(2):29. https://doi.org/10.1167/iovs.65.2.29

Purpose. Bacterial keratitis (BK) is a serious ocular infection that can cause severe inflammation and corneal scarring, leading to vision loss. In this study, we aimed to investigate the involvement of ferroptosis in the pathogenesis of BK.

Methods. Transcriptome analysis was performed to evaluate ferroptosis-related gene expression in human BK corneas. Subsequently, the ferroptosis in mouse models of *Pseudomonas aeruginosa* keratitis and corneal stromal stem cells (CSSCs) were validated. The mice were treated with levofloxacin (LEV) or levofloxacin combined with ferrostatin-1 (LEV+Fer-1). CSSCs were treated with lipopolysaccharide (LPS) or LPS combined Fer-1. Inflammatory cytokines, α-SMA, and ferroptosis-related regulators were evaluated by RT-qPCR, immunostaining, and Western blot. Iron and reactive oxygen species (ROS) were measured.

Results. Transcriptome analysis revealed significant alterations in ferroptosis-related genes in human BK corneas. In the BK mouse models, the group treated with LEV+Fer-1 exhibited reduced inflammatory cytokines (MPO, TNF-α, and IFN-γ), decreased corneal scarring and α-SMA expression, and lower Fe^{3+} compared to the BK and LEV groups. Notably, the LEV+Fer-1 group showed elevated GPX4 and SLC7A11 in contrast to the BK and LEV group. In vitro, Fer-1 treatment effectively restored the alterations of ROS, Fe^{2+}, GPX4, and SLC7A11 induced by LPS in CSSCs.

Conclusions. Ferroptosis plays a crucial role in the pathogenesis of BK. The inhibition of ferroptosis holds promise for mitigating inflammation, reducing corneal scarring, and ultimately enhancing the prognosis of BK. Consequently, this study provides a potential target for innovative therapeutic strategies for BK, which holds immense potential to transform the treatment of BK.

Keywords: bacterial keratitis, corneal scarring, ferroptosis, ferrostatin-1 (Fer-1), *Pseudomonas aeruginosa* (*P. aeruginosa*)

Bacterial keratitis (BK) is a prevalent infectious corneal disease that is a leading cause of corneal blindness.[1] *Pseudomonas aeruginosa* (*P. aeruginosa*) keratitis, a predominant cause of bacterial keratitis, leads to a rapid development of suppurative keratitis. The severity can range from pain and inflammation to corneal ulceration, hypopyon, vision loss, and even perforation if left untreated.[2,3] Despite standardized treatment approaches, corneal scarring after keratitis healing remains the primary cause of visual impairment in patients with BK.[4] Hence, developing methods to minimize inflammation and scarring is crucial for visual recovery in patients with BK.

Ferroptosis plays a crucial role in bacterial infection. Several studies show that ferroptosis occurs in the bacterial infection of the lungs, periodontal ligament, and brain.[5–7] *P. aeruginosa* causes ferroptosis in bronchial epithelium by using host polyunsaturated phosphatidylethanolamines.[8] Ferroptosis has also been reported in fungal keratitis, alkali burn corneal injury, dry eye disease, poor corneal wound healing, and corneal endothelial cells in 4°C preserved corneoscleral tissues.[9–12] Ferroptosis can directly result in iron-dependent cell death by rupturing cell membranes, condensing and deforming mitochondria, and swelling cytoplasm. It can also cause inflammatory injury in tissues by activating damage-related molecular patterns in macrophages, T cells, and neutrophils.[9,13,14] However, ferroptosis has rarely been reported in patients with BK.

As a unique form of programmed cell death, ferroptosis operates through iron-dependent phospholipid peroxidation.[14,15] The hallmark biochemical features of ferroptosis include the accumulation of iron, comprising both ferrous (Fe^{2+}) and ferric (Fe^{3+}) forms, and lipid peroxidation, resulting in the generation of reactive oxygen species (ROS) that induces cell death with an inflammatory component.[14] Central to ferroptosis regulation, glutathione peroxidase 4 (GPX4) utilizes phospholipid hydroperoxides as substrates for oxidation and plays a crucial role in regulating glutathione levels to scavenge ROS.[14,15] Additionally,

solute carrier family 7 member 11 (SLC7A11), an amino acid transporter, facilitates the uptake of extracellular cysteine into cells to support glutathione synthesis, thereby influencing ferroptosis susceptibility in various cell types.[16] Notably, the loss of GPX4 and SLC7A11 contributes to the induction of ferroptosis, a process that may be further identified by the activation and upregulation of transferrin receptor (TFR), recently recognized as a potential marker of ferroptosis.[17–19]

In this study, a comprehensive analysis of ferroptosis-related gene expression was conducted in the corneas of patients with BK using transcriptomics. Subsequently, the role of ferroptosis in *P. aeruginosa* keratitis was evaluated both in vivo and in vitro. Clinical manifestations, alpha-smooth muscle actin (α-SMA), inflammatory cytokines (myeloperoxidase [MPO], TNF-α, and IFN-γ), ferroptosis-related regulators (GPX4, SLC7A11, and TFR), ROS, and iron were examined. To further elucidate the potential therapeutic implications, ferrostatin-1 (Fer-1), an inhibitor of ferroptosis, was used to treat *P. aeruginosa* keratitis and lipopolysaccharide (LPS)-induced corneal stromal stem cells (CSSCs). Through these comprehensive analyses, we aimed to unravel the involvement of ferroptosis in the pathogenesis of BK and its potential impact on disease progression and outcomes. Additionally, we sought to elucidate the therapeutic potential of targeting ferroptosis in BK therapy.

Methods

Transcriptome Analysis

The microarray transcriptome data of 7 human BK corneas (6 *Streptococcus pneumoniae* [*S. pneumoniae*]) and 1 *P. aeruginosa* keratitis) and 12 donor normal corneas were acquired from the Gene Expression Omnibus (GEO) database (https://www.ncbi.nlm.nih.gov/geo/).[20] Our data source was specifically the GSE58291 dataset from the GEO database. The analysis of ferroptosis-related genes in human corneas followed the protocol of the previous study.[10] Ferroptosis-related genes were retrieved from FerrDb (http://www.zhounan.org/ferrdb/legacy/index.html) which contains 214 genes associated with ferroptosis in Homo sapiens. Spearman's approach was utilized to verify the repeatability of the data and analyze the connection between differentially expressed genes. For graphical plotting, the ggplot package in the R software was utilized. To reduce dimensionality while retaining essential aspects of the original variables, principal component analysis (PCA) was applied to re-organize the data into a new set of variables. Differential expression analysis was conducted using the limma package in the R program, with statistical significance defined as $|\log FC| > 1.0$ and $P < 0.05$. Subsequently, to visualize the data effectively, a volcano plot and a heat map (genes included see Additional file 1, differentially expressed genes shown in Additional file 2) were generated using the ggplot tool. The R code for analysis and visualization is accessible on GitHub at the following repository: https://github.com/xxz19900/Ferroptosis-BK.

Establishment of Bacterial Keratitis Mouse Models and Intervention

Animals. Sixty female C57BL/6 mice (aged 6–8 weeks) were obtained from Beijing Vital River Laboratory Animal Technology Co., Ltd. The mice were acclimatized in a pathogen-free environment and provided with standard rodent chow. All animal procedures were conducted in strict adherence to the guidelines set forth by the Association for Research in Vision and Ophthalmology Statement for the Use of Animals in Ophthalmic and Vision Research.

Bacterial Culture and Infection. *P. aeruginosa* was isolated from the cornea of a patient with keratitis who visited Beijing Tongren Hospital. Subsequently, *P. aeruginosa* was cultured in the blood agar media (OXOID; Thermo Fisher Scientific, UK) at 35°C for 24 hours. A single colony was picked and prepared into a bacterial suspension with 1×10^7 colony-forming units (CFU)/mL using sterile phosphate-buffered saline (PBS). The mice corneas were infected by *P. aeruginosa* according to a previous study.[21] In brief, 3 parallel 1 mm scratches were made in the central corneas of the left eyes using a 26-gauge needle under a stereomicroscope after being anesthetized with 0.1% sodium pentobarbital. Subsequently, 5 µL of PBS containing 5.0×10^4 CFU bacteria and sterile PBS (sham group) were instilled into the scratched corneas for infection. After 24 hours of infection, the corneal smear and bacterial culture were performed to confirm the successful establishment of the BK model.

Intervention of BK Mice. The infected mice were divided into three groups: the BK group without any treatment, the levofloxacin eye drops group (LEV group), and the LEV combined with ferrostatin-1 (200 µM/mL) eye drops group (LEV+Fer-1 group; Fig. 1). Throughout 7 days, both treatment groups received their designated eye drops 4 times a day.

Corneal Examination and Scoring. Keratitis was assessed under a slit-lamp biomicroscope on days 1, 3, 5, and 7 after infection (see Fig. 1). To evaluate the integrity of the corneal epithelium, 1 µL of 0.1% liquid fluorescein disodium (Shanghai Yuanye Bio-Technology Co., Ltd., China) was carefully instilled into the conjunctival sac. Following this, corneal staining was observed and recorded using a slit-lamp biomicroscope with a cobalt blue filter. The corneal opacity was assessed using a corneal scale that incorporated 3 criteria: opacity area, opacity density, and surface regularity, with each criterion being graded on a scale from 0 to 4.[22] The area of the corneal opacity was quantified as follows: 1 = 1% to 25%; 2 = 26% to 50%; 3 = 51% to 75%; and 4 = 76% to 100%. The density of the corneal opacity was scored based on the following criterion: 1 = slight cloudiness, the outline of the iris and pupil discernable; 2 = cloudy, but the outline of the iris and pupil remain visible; 3 = cloudy, opacity not uniform; and 4 = uniform opacity. The regularity of the surface was recorded as follows: 1 = slight surface irregularity; 2 = rough surface, some swelling; 3 = significant swelling, crater or serious descemetocele formation; and 4 = perforation or descemetocele. A total score of 0 was given for a normal cornea and 12 for the worst cornea.

Tissue Collection. The mice were euthanized after corneal examinations. Subsequently, the corneas were carefully removed and stored at −80°C in the refrigerator or 4% paraformaldehyde (paraffin sections) for further experiments.

Hematoxylin-Eosin Staining. After deparaffinization and hydration, the corneal paraffin sections were performed with hematoxylin-eosin (H&E) staining. In brief, the corneal paraffin sections were incubated with hematoxylin for 5 minutes and 0.5% acid alcohol differentiation solution for 5 seconds, then washed with tap water for 3 minutes. After that, they were stained with eosin for 30 seconds.

Investigative Ophthalmology & Visual Science

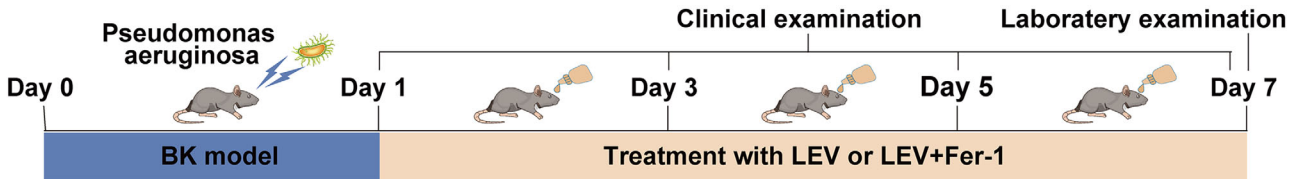

Figure 1. Schematic diagram of establishment and intervention of *P. aeruginosa* keratitis mouse models. The mice were infected by *P. aeruginosa* on day 0 and treated with LEV or LEV combined with Fer-1 from day 1 to day 7.

Corneal Stromal Stem Cell Culture and Intervention

Corneal Stromal Stem Cell Culture. With the consent of the Institutional Review Board (TRBCK2019-129), donor human sclerocorneal tissues were procured from the Beijing Tongren Eye Bank (Beijing, China) and all procedures followed the Declaration of Helsinki. Before the experiments, the tissues were immersed in Optisol-GS (Bausch & Lomb, Irvine, CA, USA). The intervals between death and preservation, as well as between death and the beginning of the experiment, were within 12 hours and 10 days, respectively.[23]

A 3 mm wide human limbal ring was used for the culture of CSSCs. After the corneal epithelium was mechanically removed, the ring was further divided into 12 pieces, with each piece placed into an individual well of a 12-well plate. The components of the CSSCs culture medium were as follows: 88% MEM Alpha basic, 10% (v/v%) fetal bovine serum, 1% penicillin/streptomycin, and 1% nonessential amino acids (100×). Primary CSSCs were obtained after being cultivated at 37°C in a 5% CO_2 atmosphere for about 14 days, with the medium changed every 2 to 3 days. Passages 3 to 6 of CSSCs were used for the subsequent experiments. Our recent study confirmed the cultivation and identification of CSSCs expressing CD90 and CD105, with the ability for adipogenesis, chondrogenesis, and osteogenesis.[23]

Intervention of Corneal Stromal Stem Cells. The CSSCs were treated with LPS (50 µg/mL) and LPS combined with Fer-1 (1 µM/mL, LPS+Fer-1 group) for 48 hours at 37°C in a 5% CO_2 atmosphere. The CSSCs treated with the culture medium without LPS and Fer-1 were used as the control group. Following the treatment period, cells from the three groups were collected for further experiments.

ROS and Iron Analysis

ROS Analysis in CSSCs. ROS was detected by using an Image-iT LIVE Green Reactive Oxygen Species Detection Kit (Invitrogen, Life Technologies, Carlsbad, CA, USA) following the manufacturer's instructions. After being treated with LPS or LPS+Fer-1 for 48 hours, the CSSCs were gently washed once with warm HBSS/Ca/Mg. Subsequently, CSSCs were incubated with 25 µM carboxy-H2DCFDA working solution at 37°C for 30 minutes in a dark room. Following the incubation, CSSCs were washed three times with HBSS/Ca/Mg and immediately observed under a fluorescence microscope to visualize the presence of ROS.

Iron Analysis in Corneal Tissues and CSSCs. Fe^{3+} in corneal tissues was detected by the Prussian Blue Iron Stain Kit (Solarbio, Beijing, China) according to the instructions. In brief, the corneal paraffin sections were incubated with Perls Working Solution at 37°C for 20 minutes. Next, the sections were exposed to an incubation solution, and enhanced working solution at 37°C for 15 minutes, respectively. Finally, the corneal sections were treated with a redyeing solution. Fe^{3+} levels were assessed by determining the percentage of positive area in corneas using ImageJ software (National Institutes of Health, Bethesda, MD, USA). The detection of Fe^{2+} in CSSCs was carried out using a FerroOrange fluorescent probe (Dojindo, Kumamoto, Japan) following the manufacturer's protocol.[24] The CSSCs subjected to the treatment were incubated with 250 µM FerroOrange at 37°C for 30 minutes, after which they were immediately observed under a fluorescence microscope.

Molecular and Protein Analysis

Antibodies. For immunohistochemistry, immunofluorescence, and Western blot, the following antibodies were used according to the manufacturers' instructions: mouse anti-TNF alpha (TNF-α, ab1793; Abcam), rabbit anti-IFN-γ (bs-0480R; Bioss), anti-MPO (22225-1-AP; Proteintech), anti-alpha smooth muscle actin (α-SMA, ab124964; Abcam), anti-transferrin receptor (TFR; ab214039; Abcam), anti-GPX4 (ab125066; Abcam), anti-SLC7A11 (PA1-16893; Invitrogen), anti-GAPDH (60004-1-Ig; Proteintech), goat anti-rabbit IgG H&L (HRP; ab205718; Abcam), HRP-conjugated affinipure goat anti-mouse IgG (H+L; SA00001-1; Proteintech), and goat anti-rabbit IgG H&L (Alexa Fluor 488; ab150077; Abcam) antibodies.

RNA Extraction and RT-qPCR. Total RNA was extracted from the corneas and CSSCs using the RNA Easy Fast Tissue/Cell Kit (Tiangen, Beijing, China). Subsequently, the RNA was reversed transcribed (RT) into cDNA using the HiScript III All-in-One RT SuperMix (Vazyme, Nanjing, China). Real-time quantitative PCR (qPCR) was performed using Tag Pro Universal SYBR qPCR Master Mix (Vazyme, Nanjing, China) on an ABI 7500 system (Applied Biosystems, USA). The qPCR process consisted of an initial step at 95°C for 30 seconds, followed by 40 cycles of denaturation at 95°C for 10 seconds, and annealing and extension at 60°C for 30 seconds. The relative expression of the mRNA was calculated using the $2^{-\Delta\Delta Ct}$ method. Additional file 3 provides details of the primers used in this study.

Immunostaining. For immunohistochemistry (IHC) staining, corneal paraffin sections were deparaffinized twice with xylene for 10 minutes each and hydrated with gradient alcohol. Next, heat-mediated antigen retrieval was then conducted. To block endogenous peroxidase, 3% hydrogen peroxide was applied for 10 minutes, and, subsequently, the paraffin sections were permeabilized with 0.1% Triton X-100 for 20 minutes and blocked with goat serum for 1 hours at room temperature. After that, the paraffin sections were incubated with MPO (1:500), TNF-α (1:250), IFN-γ (1:200),

α-SMA (1:1000), TFR (1:500), GPX4 (1:250), and SLC7A11 (1:250) antibodies overnight at 4°C. Finally, the samples were incubated with goat anti-rabbit IgG H&L (HRP) or HRP-conjugated affinipure goat anti-mouse IgG (H+L) antibodies (1:1000) for 1 hour at room temperature and stained with DAB (ZSGB-BIO, Beijing, China) for 5 to 10 minutes and observed under a microscope. The percentage of the positive area and the mean optical density were calculated using ImageJ software.

For immunofluorescence (IF) staining, CSSCs, after treatment, were fixed in 4% paraformaldehyde at room temperature for 10 minutes. Then, CSSCs were incubated with α-SMA (1:500) antibody overnight at 4°C. Negative control was incubated without any primary antibody. The paraffin sections and CSSCs were incubated with goat anti-rabbit antibody (Alexa Fluor 488; 1:1000) for 1 hour at room temperature, followed by staining with DAPI and observed under a fluorescence microscope.

Western Blot. Western blot was performed using a method in a previous study.[25] Equal amounts of proteins were electrophoresed on 10% PAGE gel and transferred to polyvinylidene fluoride membranes using a wet transfer system. Next, the membranes were blocked with 5% skim milk at room temperature for 1 hour and incubated with α-SMA (1:1000), TFR (1:1000), GPX4 (1:1000), SLC7A11 (1:1000), and GAPDH (1:20000) antibodies overnight at 4°C. After thrice washes with Tris-buffered saline with Tween-20, the membranes were incubated with goat anti-rabbit IgG H&L (HRP; 1:5000) and HRP-conjugated affinipure goat anti-mouse IgG (H+L; 1:5000) antibodies at room temperature for 1 hour. The results were detected using enhanced chemiluminescence (Analysis Quiz, Beijing, China). Protein bands were quantified using ImageJ software, with normalization to GAPDH levels for all samples.

Statistical Analysis

Statistical analyses were conducted using Prism software (version 9.0; GraphPad Software Inc., San Diego, CA, USA). The normality of quantitative data was assessed using the Shapiro-Wilk test. Differences in continuous variables between the two groups were evaluated using Student's *t*-test or Mann-Whitney test, as appropriate. While among the three groups, the one-way ANOVA or Kruskal-Wallis test was used. A value of $P < 0.05$ was considered to indicate statistical significance.

Results

Transcriptome Analysis Revealed the Occurrence of Ferroptosis in Human Corneas of BK

Transcriptome analysis was performed in 7 human corneas with BK and 12 normal cadaver corneas. PCA showed that the BK and normal corneas can be clustered into two distinct groups across all samples (Fig. 2A). Compared with the normal corneas, there were 927 upregulated genes and 687 downregulated genes in the BK corneas (Fig. 2B). Notably, significant changes were observed in ferroptosis-related genes in the BK corneas, including iron metabolism, lipid metabolism, oxidant-reductant, and endosomal sorting complexes required for transport (ESCRT)-III (Fig. 2C). Specifically, the gene expressions of iron metabolism (*ALOX5*, *FTL*, *IREB2*, and *NCOA4*), lipid metabolism (*ACSL4*), and oxidant-reductant (*SAT1*, *SOCS1*, and *TP53*) showed

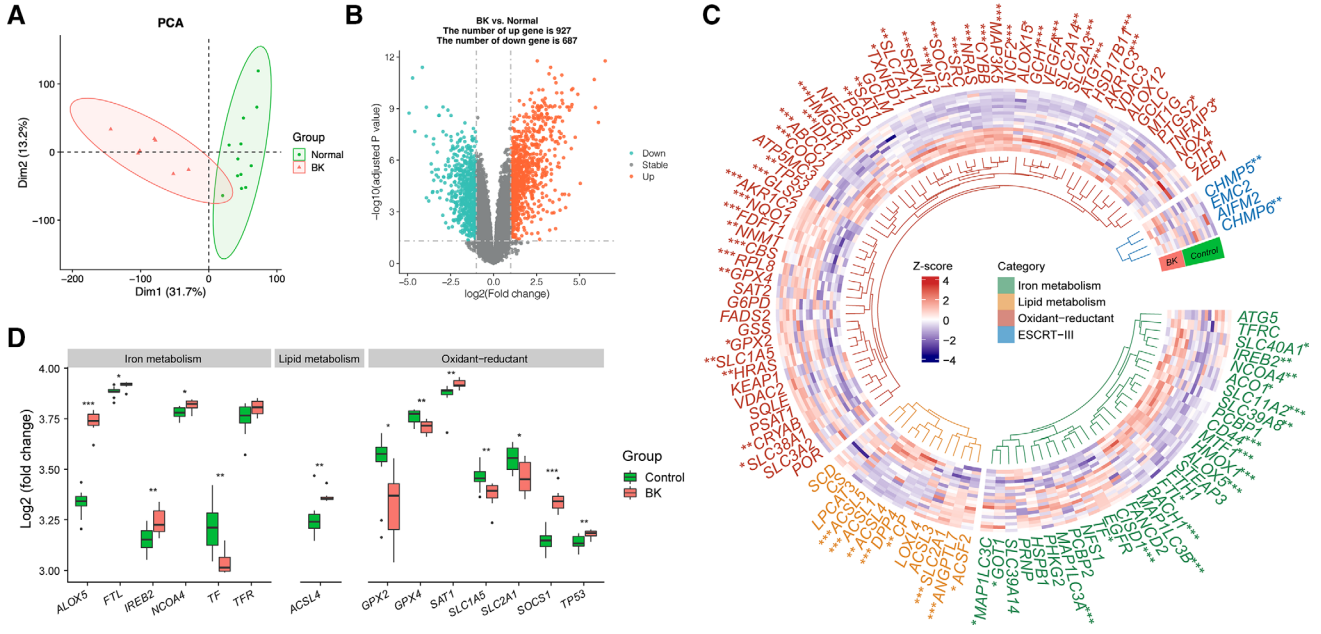

Figure 2. Ferroptosis presented in human BK corneas by transcriptome analysis. (**A**) PCA of all samples in the BK group ($n = 7$) and control group ($n = 12$). (**B**) The volcano plot indicated the up and downregulated genes in the BK group. (**C**) The heatmap showed normalized expression of genes related to iron and lipid metabolism, oxidant-reductant, and ESCRT-III of all samples. All expressions were normalized by Z-score. *Red* denoted high expression and *blue* the opposite. (**D**) Expression of classic ferroptosis-related genes in the BK group. ***$P < 0.001$; **$P < 0.01$; *$P < 0.05$.

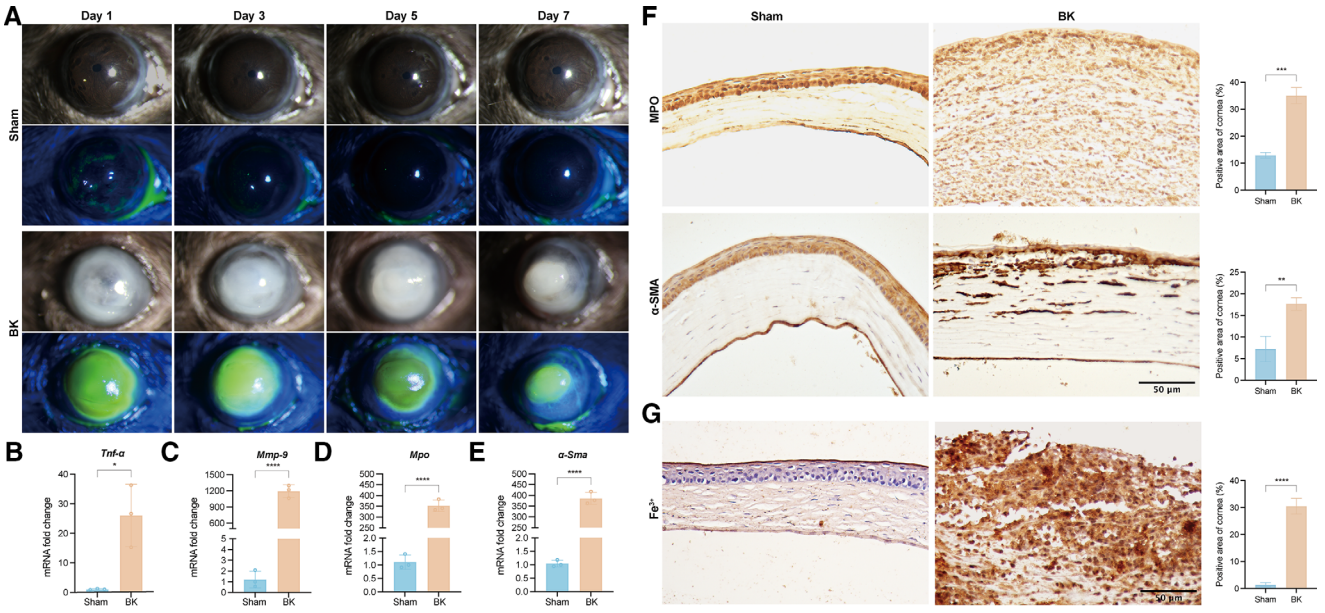

Figure 3. BK mice displayed inflammation, corneal scarring, and iron accumulation. (**A**) Corneal photographs indicated strong inflammation and corneal ulcers after being infected by *P. aeruginosa*. Upregulated of (**B**) *Tnf-α*, (**C**) *Mmp-9*, (**D**) *Mpo*, and (**E**) *α-Sma* mRNA expression in the BK group. (**F**) IHC and its quantitative analysis showed increased protein of MPO and α-SMA in cornea tissues of the BK group. (**G**) Accumulation of Fe^{3+} in corneal tissues of the BK group. ****$P < 0.0001$; ***$P < 0.001$; **$P < 0.01$; *$P < 0.05$.

an increase, while the gene expressions of transferrin (*TF*) and oxidant-reductant (*GPX2*, *GPX4*, *SLC1A5*, and *SLC2A1*) displayed a decrease in the BK corneas (all $P < 0.05$; Fig. 2D). These findings suggested that ferroptosis occurred in human corneas of patients with BK.

Ferroptosis Presented in BK Mouse Models

After being infected by *P. aeruginosa*, the mice exhibited corneal ulcers and strong inflammatory reactions on days 1, 3, 5, and 7 (Fig. 3A). The BK group showed significantly higher mRNA levels of *Tfn-α*, *Mmp-9*, *Mpo*, and *α-Sma* compared to the sham group ($P = 0.0147$, $P < 0.0001$, $P < 0.0001$, and $P < 0.0001$, respectively; Figs. 3B–3E). Moreover, IHC indicated increased protein of MPO and α-SMA in the corneas of the BK group compared to the sham group ($P = 0.0003$ and $P = 0.0053$, respectively; Fig. 3F). Interestingly, the Prussian blue iron stain showed that the BK group also had increased Fe^{3+} ($P < 0.0001$; Fig. 3G).

Fer-1 Alleviated Corneal Inflammation and Scarring in BK Mouse Models

Following treatment with LEV+Fer-1, the BK mice exhibited significantly decreased corneal clinical scores on days 3, 5 and 7 compared to those without treatment (8.5 ± 1.0 vs. 11.0 ± 0.7, $P = 0.0023$; 6.8 ± 1.7 vs. 11.0 ± 0.7, $P = 0.0003$; and 5.3 ± 1.5 vs. 11.4 ± 0.9, $P = 0.0006$, respectively; Figs. 4A, 4C) and on days 5 and 7 compared to those treated with LEV alone (6.8 ± 1.7 vs. 8.8 ± 1.2, $P = 0.046$; and 5.3 ± 1.5 vs. 8.6 ± 2.3, $P = 0.025$, respectively; Fig. 4C). Moreover, the LEV+Fer-1 group displayed smaller areas of scar and lighter opacity than that of the BK and LEV groups (Figs. 4A, 4B). Compared with the BK and LEV groups, H&E staining showed decreased infiltrated inflammatory cells in the LEV+Fer-1 group (Fig. 4D).

Fer-1 Attenuated Inflammatory Cytokines, Fibrosis, and Inhibited Ferroptosis in BK Mouse Models

The LEV+Fer-1 group exhibited decreased mRNA levels of *Mpo*, *Tnf-α*, *Ifn-γ*, and *α-Sma* compared to the BK group (all $P < 0.05$; Figs. 5A–5D). Then, the LEV+Fer-1 group had lower mRNA levels of *Mpo*, and *α-Sma* than that of the LEV group ($P = 0.049$ and $P = 0.0002$, respectively; see Figs. 5A, 5D). IHC indicated that the LEV+Fer-1 group had a lower percentage positive area of MPO, TNF-α, IFN-γ, and α-SMA in corneas than that of the BK and LEV group (all $P < 0.05$; Fig. 5E).

A higher mRNA expression of *Gpx4* in the LEV+Fer-1 group was observed compared with the BK and LEV groups (all $P < 0.0001$; Fig. 6A). The LEV+Fer-1 group had higher mRNA expression of *Slc7a11* than that of the BK group but not the LEV group ($P = 0.0228$ and $P = 0.0935$, respectively; see Fig. 6A). The mRNA level of *Tfr* was the highest in the LEV group, followed by the BK group, and the lowest in the LEV+Fer-1 group (all $P < 0.001$; see Fig. 6A). In addition, Western blot showed increased protein levels of GPX4, and SLC7A11 in the corneas of the LEV+Fer-1 group (all $P < 0.01$; Fig. 6B). Furthermore, IHC indicated that the LEV+Fer-1 group had a higher mean optical density of GPX4, and SLC7A11 than that of the BK and LEV groups (all $P < 0.05$; Fig. 6C). There was no significant difference in the mean optical density of TFR among the three groups ($P = 0.5991$; see Fig. 6C). Prussian blue iron stain showed that the percentage of the positive area of Fe^{3+} was lower than that of the BK and LEV groups ($P < 0.0001$ and $P = 0.0105$, respectively; Fig. 6D).

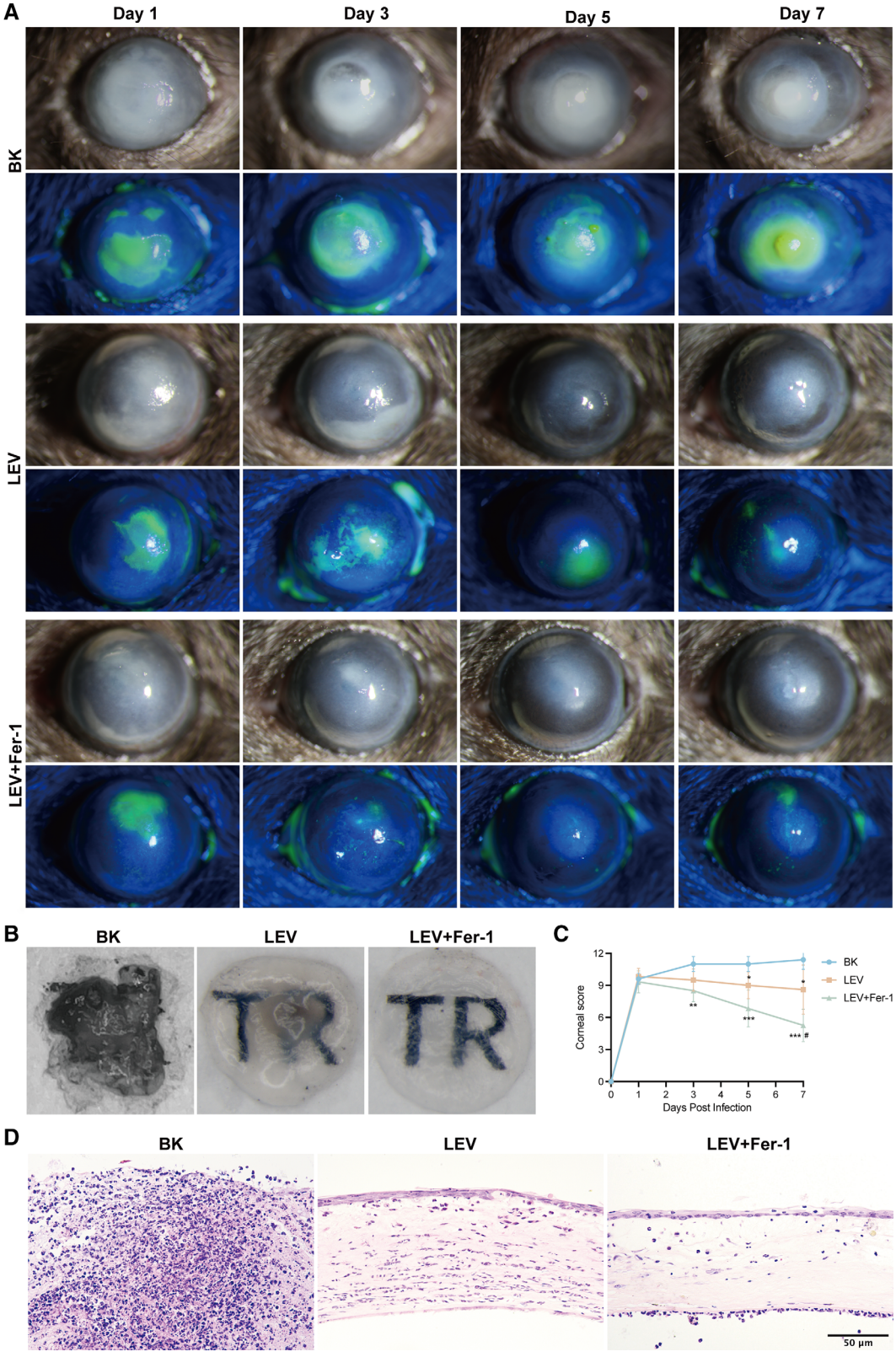

Figure 4. Fer-1 alleviated the clinical manifestation of BK mice. (**A**) Corneal photographs under diffuse and cobalt blue light after different treatments on days 1, 3, 5, and 7. (**B**) Corneal opacity evaluation for the BK, LEV, and LEV+Fer-1 groups on day 7. (**C**) Comparison of corneal scores following various treatments. (**D**) H&E staining revealed a reduction in inflammatory cells in the cornea of the LEV+Fer-1 group compared to the BK and LEV groups. * Indicates a significant difference compared to the BK group, # indicates a significant difference compared to the LEV group. ***$P < 0.001$, **$P < 0.01$, *$P < 0.05$, # $P < 0.05$.

Investigative Ophthalmology & Visual Science

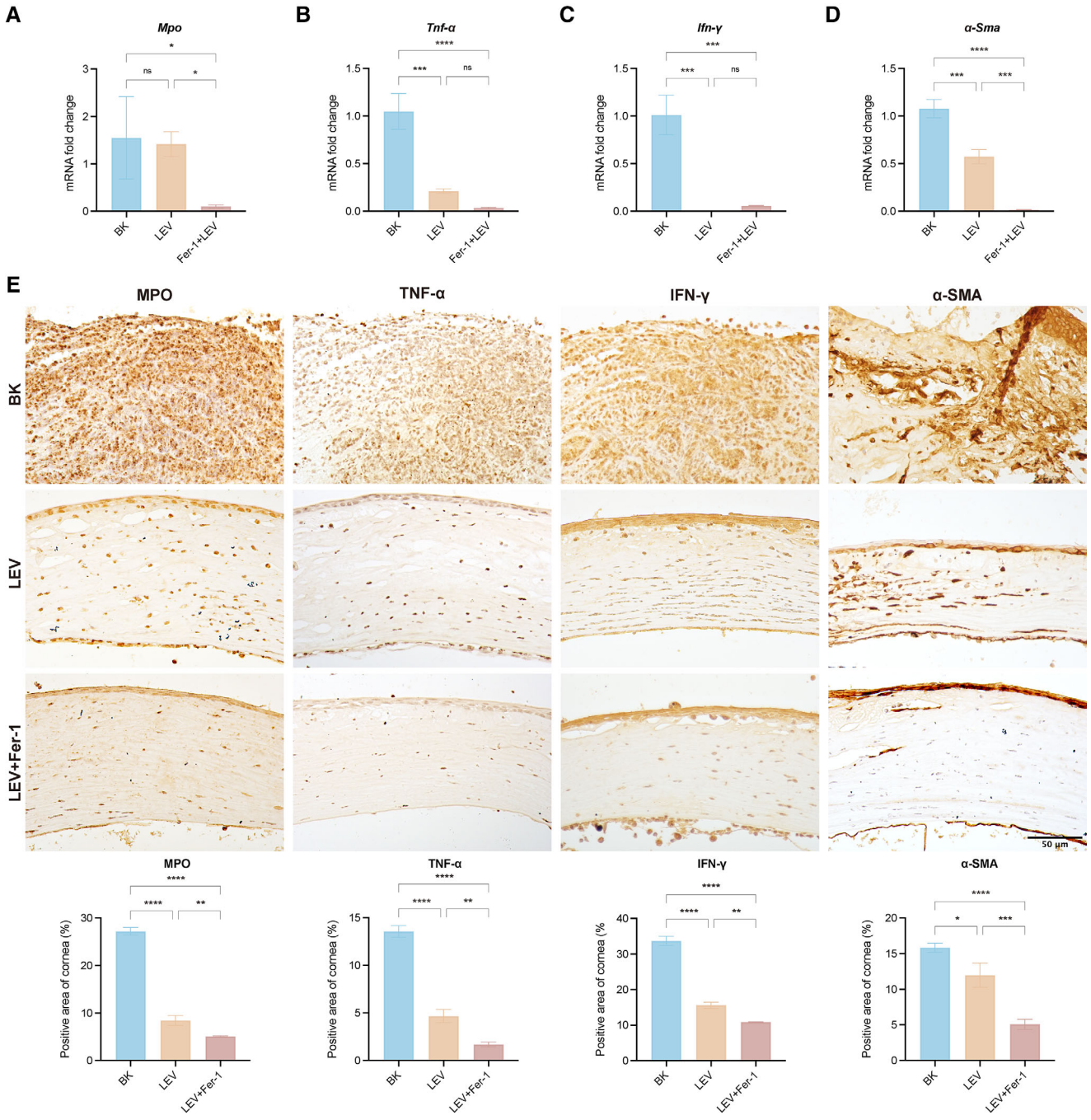

Figure 5. Fer-1 alleviated inflammatory cytokines and fibrosis of corneas in BK mice. Decreased gene expression of (**a**) *Mpo*, (**B**) *Tnf-α*, (**C**) *Ifn-γ*, and (**D**) *α-Sma* in the LEV+Fer-1 group. (**E**) IHC and its quantitative analysis showed decreased protein levels of MPO, TNF-α, IFN-γ, and α-SMA in cornea tissues of the LEV+ Fer-1 group. ****$P < 0.0001$, ***$P < 0.001$, **$P < 0.01$, *$P < 0.05$; ns, not significant.

Fer-1 Inhibited Fibrosis and Ferroptosis of CSSCs Induced by LPS

Following treatment with LPS, the levels of ROS, Fe^{2+}, and α-SMA increased, whereas GPX4 and SLC7A11 decreased (all $P < 0.05$, respectively; Fig. 7). Fer-1 treatment decreased ROS, Fe^{2+}, and α-SMA expressions in LPS-induced CSSCs ($P < 0.0001$; see Figs. 7A, 7B, 7F). Furthermore, Fer-1 also elevated the mRNA expression and protein of GPX4 and SLC7A11 in CSSCs ($P = 0.0016$ and $P = 0.0012$, respectively; see Figs. 7C, 7D), subsequently inhibiting ferroptosis. Additionally, LPS elevated the mRNA expression of *TFR* in CSSCs, although it did not have a corresponding effect on the protein levels. Fer-1 demonstrated a dual effect by reducing both the mRNA expression and protein levels of TFR ($P = 0.0012$ and $P = 0.003$, respectively; see Figs. 7E, 7F).

Discussion

BK is a severe vision-threatening infectious disease, primarily due to its severe inflammation and corneal scarring. Unfortunately, effective treatments to reduce corneal scar-

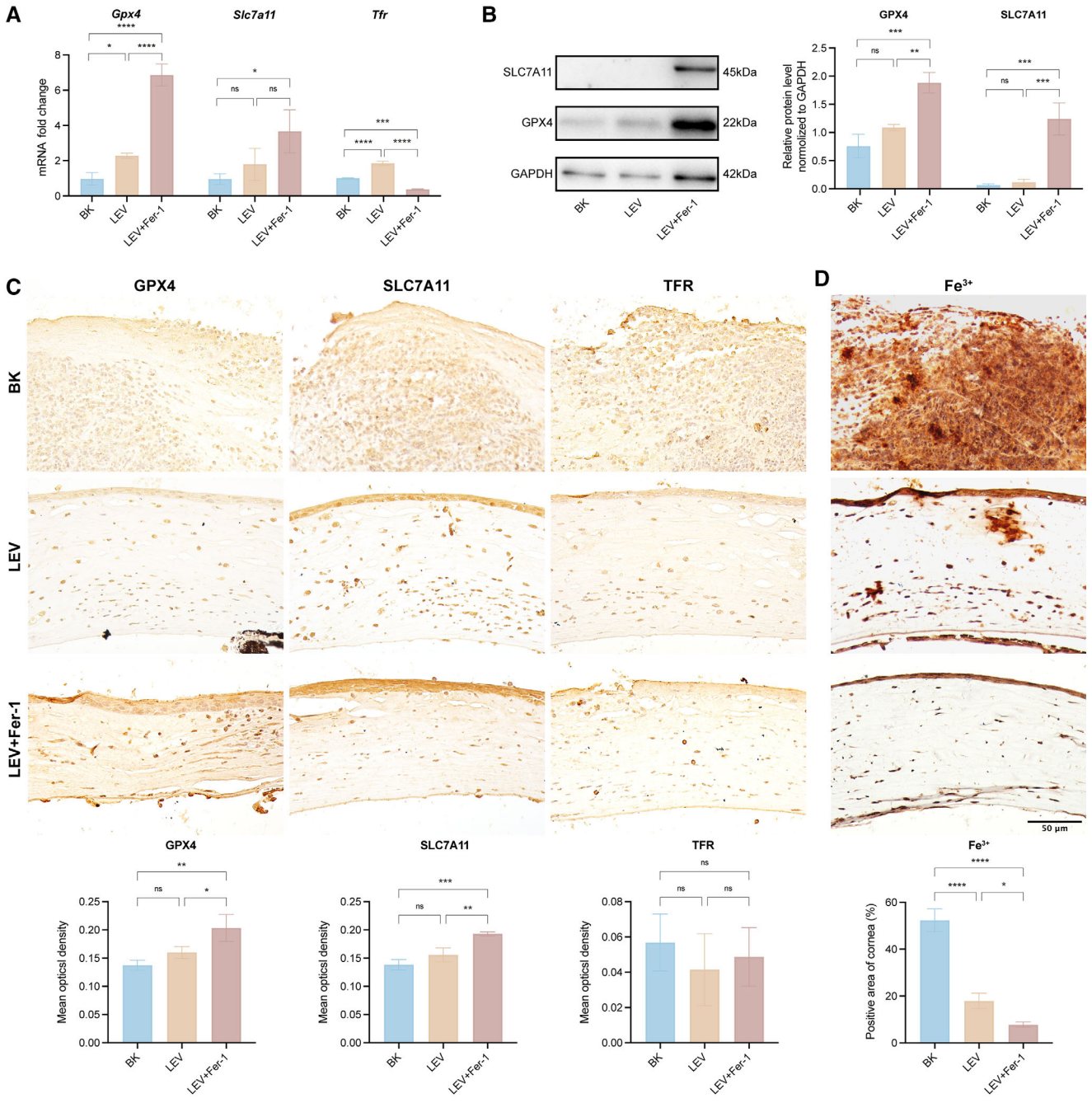

Figure 6. Fer-1 inhibited corneal ferroptosis of BK mice. (**A**) Increased gene expression of *Gpx4*, *Slc7a11*, and decreased expression of *Tfr* in the LEV+ Fer-1 group. (**B**) Western blot and its quantitative analysis showed increased protein levels of GPX4 and SLC7A11 in the LEV+ Fer-1 group. (**C**) IHC and its quantitative analysis showed decreased protein expression of GPX4 and SLC7A11 in corneal tissues of the LEV+ Fer-1 group, and no difference in TFR protein expression among the three groups. (**D**) Prussian blue iron stain showed decreased Fe^{3+} in corneal tissues of the LEV+ Fer-1 group. $^{****}P < 0.0001$; $^{***}P < 0.001$; $^{**}P < 0.01$; $^{*}P < 0.05$; ns, not significant.

ring are currently lacking. To address this, transcriptome analysis was conducted in human BK corneas, which revealed the presence of a process called ferroptosis in human corneas affected by bacteria. This finding prompted us to investigate it further with the BK mouse model. Based on the BK mice, the occurrence of ferroptosis was confirmed and ferroptosis inhibitor (Fer-1) combined with LEV could have positive effects on BK, including improvement of clinical manifestations, and reduction of corneal scarring, inflammatory cytokines, and ferroptosis. These promising results were consistent in LPS-induced CSSCs in vitro as well. Based on these compelling findings, we propose that targeting ferroptosis could represent a potential therapeutic strategy for addressing inflammation and corneal scarring in BK.

In this research, ferroptosis was observed in both human and mouse corneas affected by bacteria. We identified significant differences in ferroptosis regulators related to

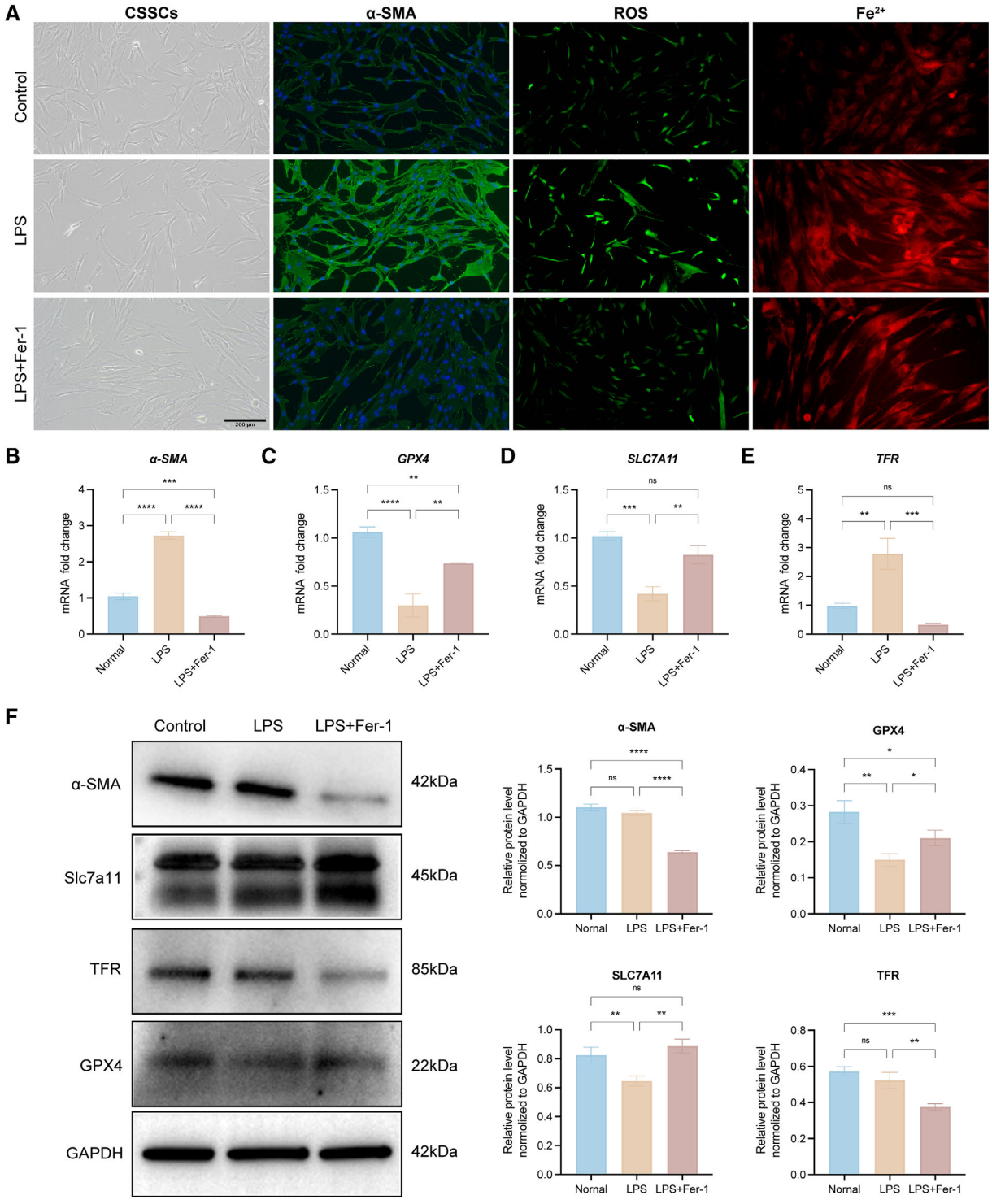

Figure 7. Fer-1 inhibited fibrosis and ferroptosis in CSSCs induced by LPS. (**A**) Increased of α-SMA, ROS, and Fe^{2+} in the CSSCs induced by LPS and restored by LPS+Fer-1. (**B**) Increased gene expression of *α-SMA* in the LPS group and decreased by LPS+Fer-1. Decreased gene expression of (**C**) *GPX4* and (**D**) *SLC7A11* in the LPS group and rescued by LPS+Fer-1. (**E**) Increased gene expression of *TFR* in the LPS group and restored by LPS+Fer-1. (**F**) Western blot showed decreased α-SMA and TFR, and increased GPX4 and SLC7A11 in the LPS+Fer-1 group. $^{****}P < 0.0001$; $^{***}P < 0.001$; $^{**}P < 0.01$; $^{*}P < 0.05$; ns, not significant.

iron metabolism, lipid metabolism, oxidant-reductant, and ESCRT-III in corneas with BK and normal controls. Ferroptosis is known to be regulated by various cellular metabolic pathways, including maintaining redox balance, managing iron levels, sustaining mitochondrial activity, metabolizing amino acids, lipids, and sugars, as well as being influenced by various disease-related signaling pathways.[14,26] *P. aeruginosa* triggers the production of ROS, leading to lipid

peroxidation and inflammation, contributing to tissue degradation in keratitis.[27,28] *S. pneumoniae* also induced ROS generation, oxidative stress, and inflammatory cytokines (IL-1β, IL-6, and IL-8) in both corneal tissues and human corneal epithelial cells.[29] ROS-scavenging glyco-nanoplatform has been found to promote antibacterial effects, reduce inflammation, and aid in wound healing in a rat model of BK.[30] A study by Sharma P and co-authors[31] found no significant differences in the expression of innate immune-related genes (*IL-1*α, *IL-1*β, and *IFN-*γ) between individuals infected with *S. pneumoniae* and *P. aeruginosa*, suggesting similar processes in neutrophil recruitment and activation in the cornea. However, despite these commonalities, the distinct clinical manifestations of *P. aeruginosa* and *S. pneumoniae* keratitis may be attributed to the release of different toxins, such as the type III secretion exoenzymes of *P. aeruginosa* and pneumolysin of *S. pneumoniae*.[32,33] Additionally, during the process of ferroptosis, the ESCRT-III-dependent membrane repair mechanism, activated by Ca^{2+} fluxes, has been demonstrated to counteract the speed of cell death and influence the immune responses linked with ferroptosis.[34] Decreasing of *TF*, and increasing of *ACSL4*, *TFR*, *SAT1*, *SOCS1*, and *TP53* induced ferroptosis.[35–38] Furthermore, a previous study by Yan Q et al.[39] revealed that ferroptosis regulator genes such as *SAT1*, *TF*, *SLC39A14*, *FTL*, *FTH1*, *SLC3A2*, *TP53*, and *SLC40A1* were associated with varying expression of $CD8^+$ T cells and monocytes, as indicated by transcriptome analysis. Similarly, Teng X et al.[10] used bioinformatic techniques to identify altered expressions of *HMOX1*, *CYBB*, and *ALOX5* in human *Fusarium* keratitis, indicating their potential involvement in the ferroptosis process. These findings highlight the complex and multifaceted nature of ferroptosis in the context of *P. aeruginosa* and *S. pneumoniae* keratitis.

Our studies demonstrated that inhibiting ferroptosis effectively alleviated inflammation and corneal scarring in the BK mice. Fer-1, a specific ferroptosis inhibitor, was initially identified and named by Dixon SJ and co-authors.[15] By restoring GPX4 and SLC7A11, Fer-1 enhances glutathione synthesis, scavenging ROS and preventing lipid peroxidation.[40] Fer-1 also reduces intracellular iron content and suppresses inflammatory response.[41] Interestingly, in our study, the mRNA expression of *Tfr* was increased in the BK mice and restored by Fer-1, which was inconsistent with another study,[41] but no difference in protein level. This discrepancy might signify variations in ferroptosis mechanisms between BK and other diseases, warranting further investigation. In summary, ferroptosis in BK is triggered by the downregulation of the GPX4/SLC7A11 axis, and Fer-1 acts on this axis to mitigate inflammation and scarring in BK. Fer-1 can alleviate corneal opacity, inflammation (IL-1β, IL-6, and TNF-α), and α-SMA in a mouse model of corneal alkali burn.[42] In the human corneal epithelial cell line, Fer-1 has proven effective in reducing cell death and increasing cell viability following exposure to cigarette smoke and heated tobacco products.[43] Another ferroptosis inhibitor, UAMC-3203, has also been found to accelerate corneal epithelial wound healing by stimulating cell migration in both in vivo and in vitro.[44] These findings highlight the potential of ferroptosis inhibitors as promising therapeutic candidates for mitigating inflammation and tissue damage in BK and other related conditions.

LPS stimulated fibrosis and triggered ferroptosis in CSSCs, both of which were effectively reversed by Fer-1. LPS, an endotoxin produced by Gram-negative bacteria, is associated with the progression of inflammation and subsequent formation of corneal scarring in BK.[45] CSSCs possess the capacity to develop into keratocytes and are capable of restoring collagen fibril alignment, thus upholding the transparency of the cornea.[46,47] LPS prompts an inflammatory reaction in activated corneal fibroblasts (known as keratocytes).[45] In a human bronchial epithelial cell line, the introduction of LPS decreased in the expression of both SLC7A11 and GPX4 genes and proteins, alongside an elevation in MDA, 4-HNE, and overall iron levels, and inducing ferroptosis.[48] These effects were subsequently rectified through the application of Fer-1. Furthermore, studies have demonstrated that LPS induces ferroptosis in liver and pulmonary fibrosis as well.[49,50] Notably, the administration of Fer-1 to lung fibroblasts has been found to decrease α-SMA expression and impede the process of ferroptosis.[49] Together, LPS has the potential to contribute to both fibrosis and ferroptosis in CSSCs and these can be rescued by Fer-1.

Despite that this study has yielded significant insights, several limitations need to be acknowledged. First, the sample size utilized in this study was relatively small, which calls for studies with larger cohorts to validate and strengthen the observed results. Second, it is crucial to note that our study specifically focused on *P. aeruginosa* and *S. pneumoniae* keratitis in humans, as well as *P. aeruginosa* in mice and CSSCs. Future investigations should explore the role of ferroptosis in keratitis caused by *S. pneumoniae* and other bacterial strains in animal models and in vitro. Last, the corneal permeability, maintenance time, and potential toxicity of ferroptosis inhibitors require further investigation to ensure their safety and efficacy during clinical applications.

In conclusion, this study highlights the significant role of ferroptosis in the pathogenesis of BK. The inhibition of ferroptosis can potentially ameliorate inflammation and corneal scarring, improving the prognosis of BK. These findings introduce a novel therapeutic target for effectively treating inflammation and corneal scarring among patients with BK.

Acknowledgments

The authors thank Zhibao Zhang (Beijing Institute of Ophthalmology, Beijing Tongren Hospital, Capital Medical University) for preparing tissue sections for histopathology.

Supported by the National Natural Science Foundation of China (grant no. 81970765 to Q.L.).

Author Contributions: Q. Chen, L. Wang, and Y. Wei performed the experiments. Q. Chen analyzed the data and wrote the manuscript. X. Xu performed the bioinformatics analysis. X. Guo revised the manuscript. Q. Liang designed the experiment, provided materials, and revised the paper. All authors read and approved the final manuscript.

Data Availability Statement: Additional data and materials supporting the findings of this study are available from the corresponding author upon request.

Disclosure: **Q. Chen**, None; **L. Wang**, None; **Y. Wei**, None; **X. Xu**, None; **X. Guo**, None; **Q. Liang**, None

References

1. Jadi PK, Dave A, Issa R, et al. Tetraspanin CD9-derived peptides inhibit Pseudomonas aeruginosa corneal infection and aid in wound healing of corneal epithelial cells. *Ocul Surf*. 2023;S1542-0124(23):00087–00093.

2. Wang H, Song F, Feng J, et al. Tannin coordinated nanozyme composite-based hybrid hydrogel eye drops for prophylactic treatment of multidrug-resistant Pseudomonas aeruginosa keratitis. *J Nanobiotechnology*. 2022;20(1):445.
3. Enzor R, Bowers EMR, Perzia B, et al. Comparison of clinical features and treatment outcomes of Pseudomonas aeruginosa keratitis in contact lens and non-contact lens wearers. *Am J Ophthalmol*. 2021;227:1–11.
4. Ray KJ, Srinivasan M, Mascarenhas J, et al. Early addition of topical corticosteroids in the treatment of bacterial keratitis. *JAMA Ophthalmol*. 2014;132(6):737–741.
5. Wang Y, Wang L, Sun T, et al. Study of the inflammatory activating process in the early stage of Fusobacterium nucleatum infected PDLSCs. *Int J Oral Sci*. 2023;15(1):8.
6. Qiang L, Zhang Y, Lei Z, et al. A mycobacterial effector promotes ferroptosis-dependent pathogenicity and dissemination. *Nat Commun*. 2023;14(1):1430.
7. Chen J, Li T, Zhou N, et al. Engineered Salmonella inhibits GPX4 expression and induces ferroptosis to suppress glioma growth in vitro and in vivo. *J Neurooncol*. 2023;163(3):607–622.
8. Dar HH, Tyurina YY, Mikulska-Ruminska K, et al. Pseudomonas aeruginosa utilizes host polyunsaturated phosphatidylethanolamines to trigger theft-ferroptosis in bronchial epithelium. *J Clin Invest*. 2018;128(10):4639–4653.
9. Guo XX, Pu Q, Hu JJ, Chang XJ, Li AL, Li XY. The role of regulated necrosis in inflammation and ocular surface diseases. *Exp Eye Res*. 2023;233:109537.
10. Teng X, Xiong X, Sha X, et al. Identification of hub genes and pathways of ferroptosis in Fusarium keratitis by bioinformatics methods. *Front Cell Infect Microbiol*. 2023;13:1103471.
11. Liu X, Cui Z, Chen X, et al. Ferroptosis in the lacrimal gland is involved in dry eye syndrome induced by corneal nerve severing. *Invest Ophthalmol Vis Sci*. 2023;64(7):27.
12. Skeie JM, Aldrich BT, Nishimura DY, et al. Ubiquinol supplementation of donor tissue enhances corneal endothelial cell mitochondrial respiration. *Cornea*. 2020;39(10):1285–1290.
13. Vanden Berghe T, Linkermann A, Jouan-Lanhouet S, Walczak H, Vandenabeele P. Regulated necrosis: the expanding network of non-apoptotic cell death pathways. *Nat Rev Mol Cell Biol*. 2014;15(2):135–147.
14. Tang D, Chen X, Kang R, Kroemer G. Ferroptosis: molecular mechanisms and health implications. *Cell Res*. 2021;31(2):107–125.
15. Dixon SJ, Lemberg KM, Lamprecht MR, et al. Ferroptosis: an iron-dependent form of nonapoptotic cell death. *Cell*. 2012;149(5):1060–1072.
16. Lei G, Zhang Y, Koppula P, et al. The role of ferroptosis in ionizing radiation-induced cell death and tumor suppression. *Cell Res*. 2020;30(2):146–162.
17. Feng H, Schorpp K, Jin J, et al. Transferrin receptor is a specific ferroptosis marker. *Cell Rep*. 2020;30(10):3411–3423.e3417.
18. Zhao Y, Zhang H, Cui JG, et al. Ferroptosis is critical for phthalates driving the blood-testis barrier dysfunction via targeting transferrin receptor. *Redox Biol*. 2023;59:102584.
19. Badgley MA, Kremer DM, Maurer HC, et al. Cysteine depletion induces pancreatic tumor ferroptosis in mice. *Science*. 2020;368(6486):85–89.
20. Chidambaram JD, Kannambath S, Srikanthi P, et al. Persistence of innate immune pathways in late stage human bacterial and fungal keratitis: results from a comparative transcriptome analysis. *Front Cell Infect Microbiol*. 2017;7:193.
21. Cui X, Gao N, Me R, Xu J, Yu FX. TSLP protects corneas from pseudomonas aeruginosa infection by regulating dendritic cells and IL-23-IL-17 pathway. *Invest Ophthalmol Vis Sci*. 2018;59(10):4228–4237.
22. Wu TG, Wilhelmus KR, Mitchell BM. Experimental keratomycosis in a mouse model. *Invest Ophthalmol Vis Sci*. 2003;44(1):210–216.
23. Wang L, Xu X, Chen Q, et al. Extracellular vesicle microRNAs from corneal stromal stem cell enhance stemness of limbal epithelial stem cells by targeting the Notch pathway. *Invest Ophthalmol Vis Sci*. 2023;64(12):42.
24. Zuo X, Zeng H, Wang B, et al. AKR1C1 protects corneal epithelial cells against oxidative stress-mediated ferroptosis in dry eye. *Invest Ophthalmol Vis Sci*. 2022;63(10):3.
25. Wang L, Wang X, Chen Q, et al. MicroRNAs of extracellular vesicles derived from mesenchymal stromal cells alleviate inflammation in dry eye disease by targeting the IRAK1/TAB2/NF-κB pathway. *Ocul Surf*. 2023;28:131–140.
26. Jiang X, Stockwell BR, Conrad M. Ferroptosis: mechanisms, biology and role in disease. *Nat Rev Mol Cell Biol*. 2021;22(4):266–282.
27. Deng Q, Sun M, Yang K, et al. MRP8/14 enhances corneal susceptibility to Pseudomonas aeruginosa Infection by amplifying inflammatory responses. *Invest Ophthalmol Vis Sci*. 2013;54(2):1227–1234.
28. Wang Y, Carion TW, Ebrahim AS, Sosne G, Berger EA. Adjunctive thymosin beta-4 treatment influences PMN effector cell function during pseudomonas aeruginosa-induced corneal infection. *Cells*. 2021;10(12):3579.
29. Sharma P, Roy S. Streptococcus pneumoniae exerts oxidative stress, subverts antioxidant signaling and autophagy in human corneal epithelial cells that is alleviated by tert-Butylhydroquinone. *Med Microbiol Immunol*. 2022;211(2–3):119–132.
30. Zhang Y, Li G, Zhang X, Lin L. ROS-scavenging glyconanoplatform for synergistic antibacterial and wound-healing therapy of bacterial keratitis. *J Mater Chem B*. 2022;10(24):4575–4587.
31. Karthikeyan RS, Priya JL, Leal SM, Jr., et al. Host response and bacterial virulence factor expression in Pseudomonas aeruginosa and Streptococcus pneumoniae corneal ulcers. *PLoS One*. 2013;8(6):e64867.
32. Nanayakkara U, Khan MA, Hargun DK, Sivagnanam S, Samarawickrama C. Ocular streptococcal infections: a clinical and microbiological review. *Surv Ophthalmol*. 2023;68(4):678–696.
33. Ung L, Chodosh J. Foundational concepts in the biology of bacterial keratitis. *Exp Eye Res*. 2021;209:108647.
34. Pedrera L, Espiritu RA, Ros U, et al. Ferroptotic pores induce Ca(2+) fluxes and ESCRT-III activation to modulate cell death kinetics. *Cell Death Differ*. 2021;28(5):1644–1657.
35. Wu J, Minikes AM, Gao M, et al. Intercellular interaction dictates cancer cell ferroptosis via NF2-YAP signalling. *Nature*. 2019;572(7769):402–406.
36. Hu ZW, Wen YH, Ma RQ, et al. Ferroptosis driver SOCS1 and suppressor FTH1 independently correlate with M1 and M2 macrophage infiltration in head and neck squamous cell carcinoma. *Front Cell Dev Biol*. 2021;9:727762.
37. Hong X, Roh W, Sullivan RJ, et al. The lipogenic regulator SREBP2 induces transferrin in circulating melanoma cells and suppresses ferroptosis. *Cancer Discov*. 2021;11(3):678–695.
38. Shostak K, Jiang Z, Charloteaux B, et al. The X-linked trichothiodystrophy-causing gene RNF113A links the spliceosome to cell survival upon DNA damage. *Nat Commun*. 2020;11(1):1270.
39. Yan Q, Zheng W, Jiang Y, et al. Transcriptomic reveals the ferroptosis features of host response in a mouse model of Zika virus infection. *J Med Virol*. 2023;95(1):e28386.
40. Xu Y, Li Y, Li J, Chen W. Ethyl carbamate triggers ferroptosis in liver through inhibiting GSH synthesis and suppressing Nrf2 activation. *Redox Biol*. 2022;53:102349.

Investigative Ophthalmology & Visual Science

41. Ouyang C, Ma X, Zhao J, et al. Oleanolic acid inhibits mercury chloride induced-liver ferroptosis by regulating ROS/iron overload. *Ecotoxicol Environ Saf*. 2023;258:114973.
42. Wang K, Jiang L, Zhong Y, et al. Ferrostatin-1-loaded liposome for treatment of corneal alkali burn via targeting ferroptosis. *Bioeng Transl Med*. 2022;7(2):e10276.
43. Otsu W, Ishida K, Chinen N, et al. Cigarette smoke extract and heated tobacco products promote ferritin cleavage and iron accumulation in human corneal epithelial cells. *Sci Rep*. 2021;11(1):18555.
44. Balla A, Tran B, Valtari A, et al. A novel ferroptosis inhibitor UAMC-3203, a potential treatment for corneal epithelial wound. *Pharmaceutics*. 2022;15(1):118.
45. Fukuda K, Ishida W, Fukushima A, Nishida T. Corneal fibroblasts as sentinel cells and local immune modulators in infectious keratitis. *Int J Mol Sci*. 2017;18(9):1831.
46. Kureshi AK, Funderburgh JL, Daniels JT. Human corneal stromal stem cells exhibit survival capacity following isolation from stored organ-culture corneas. *Invest Ophthalmol Vis Sci*. 2014;55(11):7583–7588.
47. Du Y, Carlson EC, Funderburgh ML, et al. Stem cell therapy restores transparency to defective murine corneas. *Stem Cells*. 2009;27(7):1635–1642.
48. Liu P, Feng Y, Li H, et al. Ferrostatin-1 alleviates lipopolysaccharide-induced acute lung injury via inhibiting ferroptosis. *Cell Mol Biol Lett*. 2020;25:10.
49. Pei Z, Qin Y, Fu X, et al. Inhibition of ferroptosis and iron accumulation alleviates pulmonary fibrosis in a bleomycin model. *Redox Biol*. 2022;57:102509.
50. Zhao W, Lei M, Li J, et al. Yes-associated protein inhibition ameliorates liver fibrosis and acute and chronic liver failure by decreasing ferroptosis and necroptosis. *Heliyon*. 2023;9(4):e15075.

Investigative Ophthalmology & Visual Science